Research Article

Synthesis of PdCu Alloy Decorated Flower-Like NiO Composite and its Catalytic Properties for Highly Efficient CO Oxidation

Feifei Wang[*], Shuchao Hao and Jinnan Li

School of Chemistry and Chemical Engineering, Henan Normal University, Xinxiang, China

[*]**Corresponding author:** Feifei Wang, School of Chemistry and Chemical Engineering, Henan Normal University, Xinxiang, 453007, P. R. China, Tel: +8615836044514, Email: wffmy@163.com

Citation: Feifei Wang, Shuchao Hao, Jinnan Li (2023) Synthesis of PdCu Alloy Decorated Flower-Like Nio Composite and its Catalytic Properties for Highly Efficient Co Oxidation. J Chem Eng Catal 2: 1-11

Abstract

Nanoscale PdCu alloy catalysts supported on flower-like NiO (F-NiO) were successfully prepared using a hydrothermal method in which ethylene glycol was used as a reductant and glutamate was employed as an additive. The characterization of X-ray diffraction (XRD), field-emission scanning electron microscopy (FE-SEM) and transmission electron microscope (TEM) suggested that the Pd_1Cu_1/ F-NiO catalysts possessed a relatively small PdCu nanoparticles (16.3nm) and hierarchical structures. These features were beneficial as a catalyst for CO oxidation. As a comparison, Pd/ F-NiO and Cu/ F-NiO were prepared under similar conditions. The catalytic activities of these catalysts for CO oxidation were also studied. The results showed that the Pd_1Cu_1/ F-NiO possess much higher activity for low temperature CO oxidation, and the CO conversion in the presence of Pd_1Cu_1/ F-NiO could reach about 83.1% even at 25°C.\

Keywords: Flower-like NiO; PdCu alloy; Catalyst; CO Oxidation

Introduction

Since the automobile amount rise in recent years, the Global has had trouble with environmental problems, air pollution in particular. Carbon monoxide is one of the main air pollutants generated from automotive emission, and catalytic oxidation is considered to be the most efficient method for elimination of carbon monoxide from environment.

Among the catalysts, the transition metal oxides with particular morphologies of micro/nano configuration have fascinated the scientific community in the recent years because of its large specific surface area and outstanding oxygen storage and release capacity [1-2]. All these have been proved to be beneficial as support for CO oxidation [3-6]. As a p-type wide band gap semiconductor, NiO is a very promising material among the transition metal oxides because of its extensive important applications as catalysts [7-9], electrode materials for lithium ion batteries and fuel cells [10,11] and magnetic materials [12]. Thus, precious metals such as gold, platinum and rhodium with high activity and stability supported on transition metal oxides have been widely used in CO oxidation and gas exhaust emissions control [13-15].

Recently, a series of transition metal oxide (ferric oxide, nickel oxide, silica, etc.) supported Pd catalysts have been synthesized and applied for low temperature CO oxidation because they are much stable and relatively less expensive than Au [16–18]. In particular, to solve the continuously rising price and rare reserve of the noble metals problems, Alloying of noble metals with non-noble metals (Fe, Co, Cu etc.) is one of the effective approaches to enhance the catalytic activity and the selectivity and thereby reduce the loading of the noble metals [19-23].

In this paper, novel flower-like nickel oxide spheres were synthesized by hydrothermal method. NiO nanosheets less than 10 nm aggregated together to form the flower-like NiO microspheres support. PdCu nanoparticles were evenly deposited by wet impregnation and in-situ reduction protocol. The resulting materials showed excellent catalytic activity for low temperature CO oxidation especially under ambient conditions.

Experimental Section

Preparation of flower-like NiO(F-NiO)

4g CTAC (cetanecyl trimethyl ammonium chloride) and 7.27g nickel nitrate hexahydrate were dissolved into 20 mL anhydrous ethanol in a 300 mL beaker, stirring until the CTAC is basically dissolved, then 80 mL deionized water at 90 °C was added into the beaker under vigorous stirring conditions. After 10 minutes, urea (1.6 wt%, 100 mL) was dropped into the mixed solution with feeding speed at 2-3 drops per second. After stirred 6 hours at room temperature, the mixture was transferred into an electro-thermostatic blast oven and aged at 90 °C for 4.5 h. The precipitate was centrifuged, washed with deionized water and anhydrous ethanol. The obtained green samples were frozen in a cryogenic refrigerator for 8 hours, and then dried in a freeze-dryer for 24 hours. The fine green $Ni(OH)_2 \cdot xH_2O$ powder was annealed under air atmosphere at 400 °C for 2h with a ramp rate of 5 °C per min to get the final product F-NiO.

Synthesis of PdCu/ F-NiO

An aqueous solution of $PdCl_2$ (3.3 mg/mL, 3.8 mL), 20 mg of $CuSO_4 \cdot 5H_2O$, and 50 mg of glutamate were mixed together in 40 mL of ethylene glycol (EG). The pH of the system was adjusted to ca. 11 by the dropwise addition of the 8 wt% KOH/EG solution under vigorous stirring. During the process, the green solution turned into dark blue. Subsequently, 30 mg of F-NiO were added, and the solution was stirred for 2 h to obtain a homogeneous suspension. Upon completion, the suspension was transferred into a 50 mL Teflon-lined stainless-steel autoclave. The autoclave was sealed, heated at 160 °C for 6 h, and air-cooled to room temperature. Finally, the product was collected by filtration and washed several times with deionized water. The obtained product was dried at 40°C under vacuum for 8 h. The catalyst thus obtained was denoted as PdCu/ F-NiO. PdCu catalysts supported on F-NiO with Pd:Cu nominal atomic ratios of 1:0, 1:1, and 0:1 were prepared under similar conditions and denoted as 2 wt% Pd/ F-NiO, 2 wt% Cu / F-NiO, and 2 wt% Pd_1Cu_1/ F-NiO, respectively.

Catalyst Characterization

The catalyst's crystallographic structure was analyzed using X-ray diffraction (XRD) (X'Pert3 Powder instrument. (PANalytical B.V.) operated at 45 kV and tube current of 40mA). The field-emission scanning electron microscopy (FE-SEM) images were conducted on a SU8010 system. The transmission electron microscope (TEM) images were obtained using a JOEL JEM-2100 operated at 200 kV. A drop of ethanol-dispersed nanoparticles was placed on a carbon-coated copper grid and left to dry. The catalysts' surface area detailed in the Brunauer–Emmett–Teller technique (BET) was measured by an ASAP2460 instrument, which was also used to obtain a nitrogen adsorption–desorption isotherm and pore diameter distribution pattern. Elemental analysis of the samples was performed using Inductively Coupled Plasma Optical Emission Spectroscopy (ICP-OES Thermo Scientific iCAP 6500 ICP Spectrometer, (Waltham, MA, USA).

CO oxidation test

The catalytic activity for CO oxidation was carried out infixed-bed quartz tubular reactor (length 220 mm, i.d. 9 mm) containing 100 mg of catalyst under a steady-state condition, involving a feed stream with a fixed composition of CO 2%, O_2 18%, and N_2 80% by volume, where N_2 was used as diluent. The sample was pretreated in an air stream at 200 °C for 3 h and then cooled to reaction temperature. After that, the mixed gases were switched on. The reaction was carried out with the same space velocity of 30000 mL g^{-1} h^{-1}. The composition of the gas exiting the reactor was monitored by online gas chromatography (GC-9160). The conversions were determined on the basis of CO consumption and CO_2 formation. All the catalytic results were repeated three times at a given temperature.
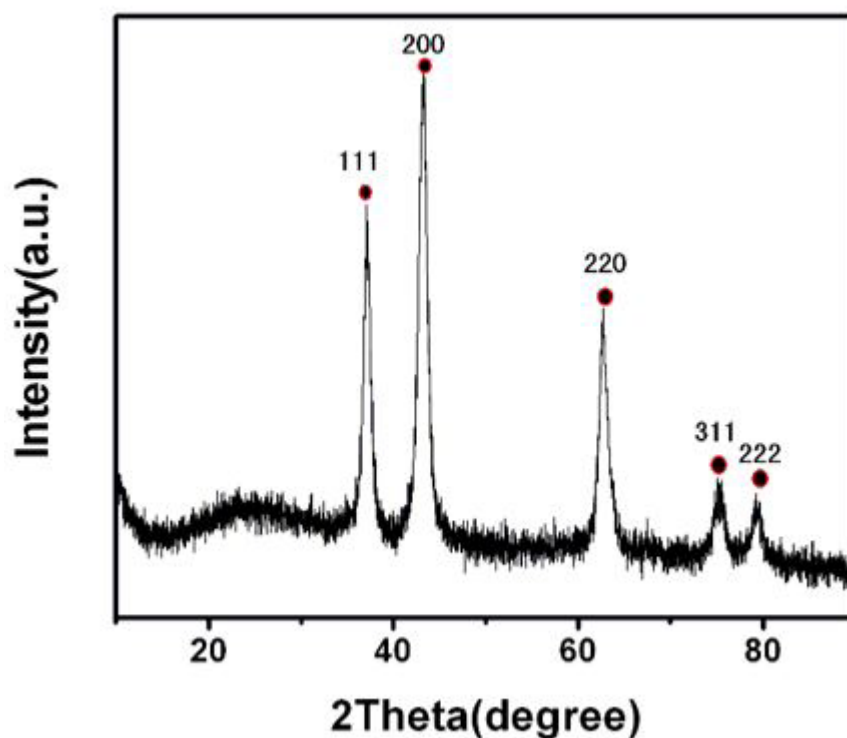
Results and Discussion

Figure 1: XRD patterns of F-NiO

Figure 1 shows the XRD patterns of F-NiO. The XRD pattern of the as-prepared flower-like NiO spheres shows well-defined diffraction feature of the face centered cubic (fcc) NiO phase. The characteristic diffraction peaks at 2θ of 37.2°, 43.3°, 62.9°, 75.4° and 79.4° could be assigned to (111), (200), (220), (311) and (222) crystal planes respectively. The positions of the corresponding peaks are in good agreement with the reported data (JCPDS Card No. 47-1049). The XRD pattern of F-NiO indicates that the Ni(OH)$_2$·xH$_2$O precursor are decomposed completely to F-NiO under the experiment conditions.
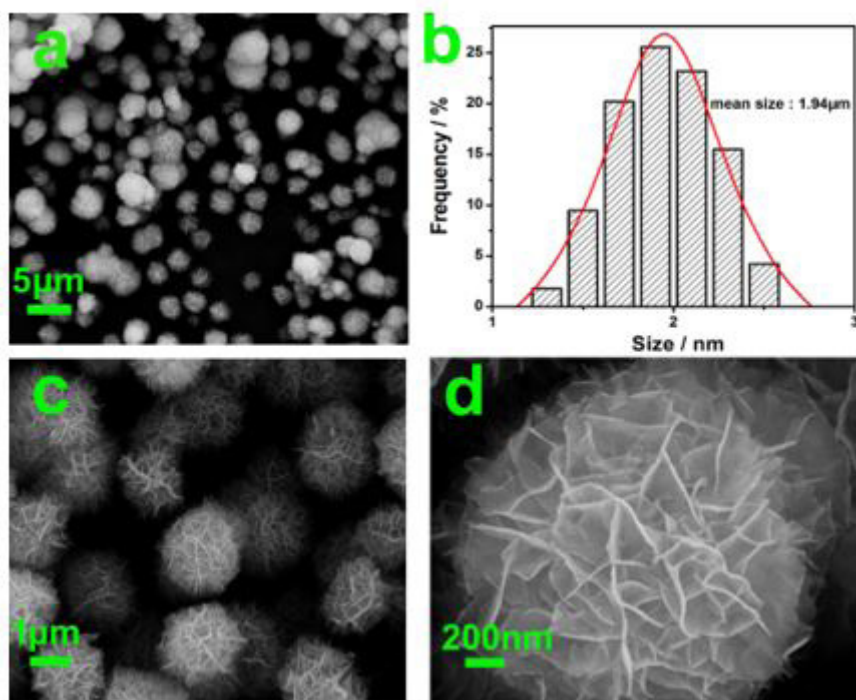
Figure 2: FE-SEM micrographs of F-NiO the F-NiO was characterized by FE-SEM-(field emission scanning electron microscopy) test, and the results are shown in Figure 2. From Figure 2a and 2c' we can see that the as-prepared NiO are the well-dispersed flower-like microspheres with average size of 1.94 μm and narrow size distribution (Figure 2b). As shown in Figure 2d the monodispersed NiO microspheres were formed by densely packed irregular assembling nanometer sheets with a thickness of about 9nm
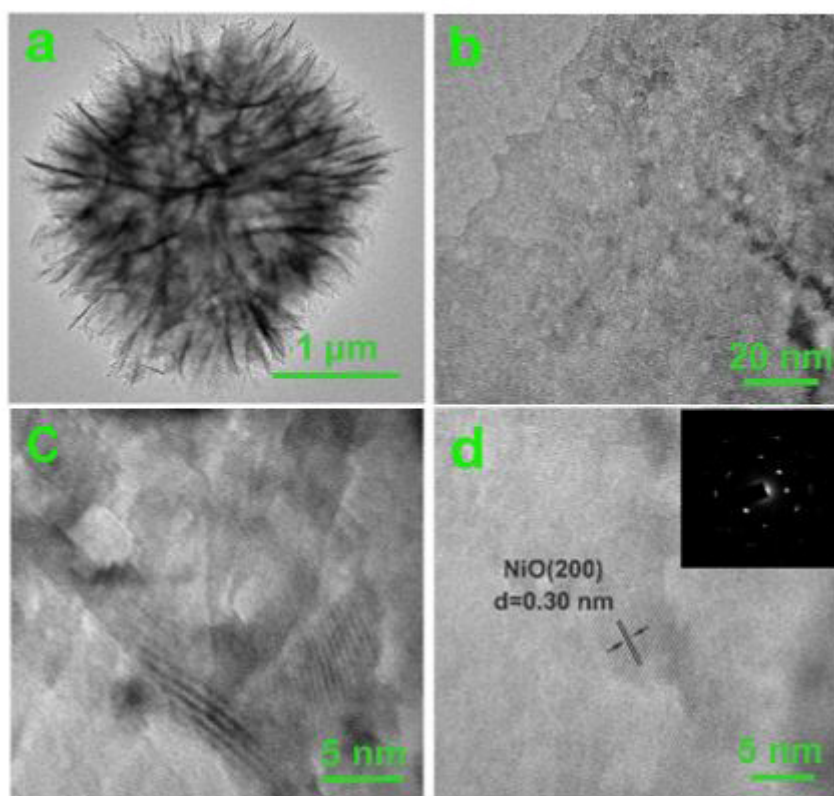

Figure 3: TEM micrographs of F-NiO

In order to further explore the inner structure of F-NiO microspheres, a series transmission electron microscopy (TEM) observations were collected. The results are shown in Figure 3. It clearly reveals that the monodisperse configuration flower-like NiO microspheres are made of the nanometer piece of interlaced assemble micron grade spherical flowers (Figure 3a). From Figure 3b and 3c, we can see that the surface structure of the nanosheet forming the NiO micron flower is not smooth and dense, but a nanosheet with a cavity structure of about 9nm in thickness. The lattice spacing in Figure 3d (d=0.30 nm, which represents the (200) crystal surface of NiO) once again proves that the calcined sample is nickel oxide. In addition, we further studied the crystal phase of NiO micron flowers with clear monodispersed configuration, and the results are illustrated in Figure 3d, which is the selective electron diffraction result of NiO flower-like structure in Figure 3d. From the test results of single point dispersion, we analyzed the NiO flower-like configuration as a single crystal system.
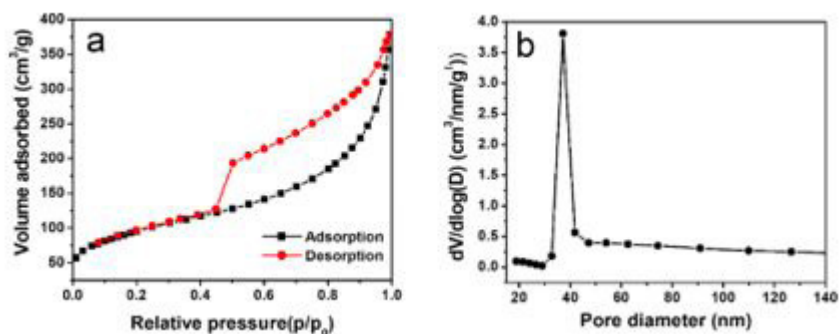

Figure 4: (a) N$_2$ adsorption/desorption isotherms and (b) BJH pore size distribution plots of flower-like NiO nanocrystals

The specific surface area and porosity of the as-prepared flower-like NiO nanocrystals were determined using N$_2$ adsorption/desorption analysis. The N$_2$ adsorption/desorption isotherms and the corresponding pore size distribution plots for F-NiO nanocrystals are shown in Figure 4. The BET surface area of the F-NiO nanocrystals is as high as 328.6m^2/g. According to the IUPAC classification, the obtained isotherm (Figure 4a) can be recognized as a type IV N$_2$ adsorption/desorption isotherm, which is the typical characteristics of mesoporous materials. Furthermore, the F-NiO nanocrystals have an obvious strong and narrow peak at about 37.1 nm calculated by Barrett–Joyner–Halenda (BJH) analysis using the desorption branch of the isotherm (Figure 4b). The results could indicate that F-NiO nanocrystals with a large BET surface area and the hierarchical architectures are beneficial to enhance the catalytic ability of catalyst.

X-Ray diffraction (XRD) results were used to demonstrate the formation of the PdCu alloy phase. Figure 5 shows the XRD patterns of Cu/F-NiO, Pd/F-NiO, and Pd$_1$Cu$_1$/F-NiO, respectively. From the XRD patterns of Figure 5, A series sharp diffraction peaks (111), (200), (220), (311) and (222) are fitted well with standard PDF card of NiO (no.47-1049). The standard peak located at 42.3° is also assigned to (111) plane of Cu in the XRD pattern for Cu/F-NiO (Figure 5a). A weak peak of catalyst with 2 wt% loading contents emerges at 2θ = 40° (Figure 5b), which corresponded to (111) diffraction bands of palladium with face-centered cubic. After loaded with palladium and copper, it can be observed that there is a slightly positive shift of the XRD peaks of Pd$_1$Cu$_1$/F-NiO compared with those of the Pd/ F-NiO (Figure 5c). The peak of PdCu alloy (111) plane lies between the Pd (40.1°) and Cu (42.3°) and the calculated lattice parameter of PdCu alloy (0.217 nm) lies between the Pd (0.225 nm) and Cu (0.209 nm), which is close to the standard d value of PdCu alloyed (111) plane distance. These results show the formation of the PdCu alloy phase. Similar phenomena, the shift of the diffraction peaks and the change of the lattice parameters during the formation of the alloy, have also been reported.
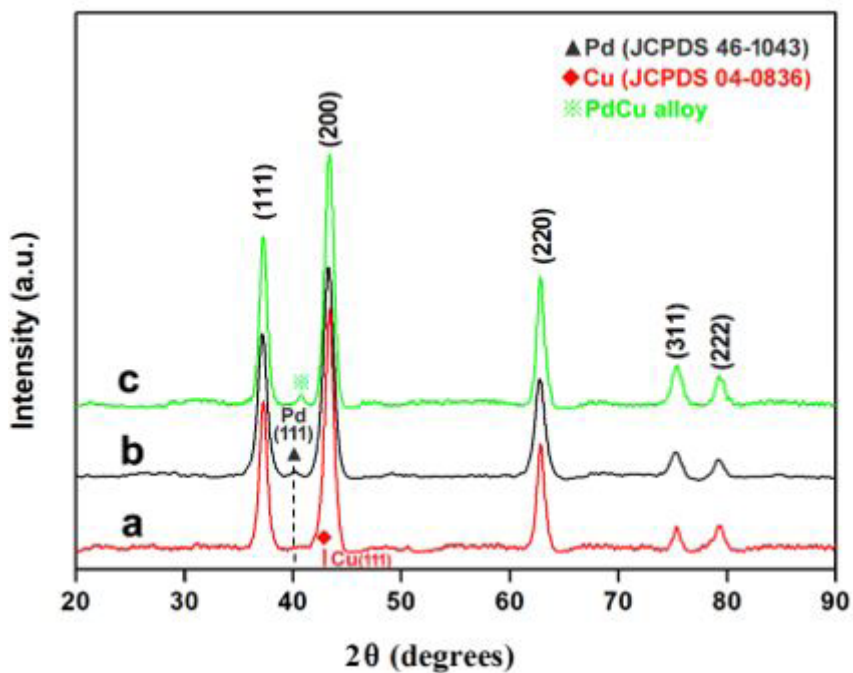
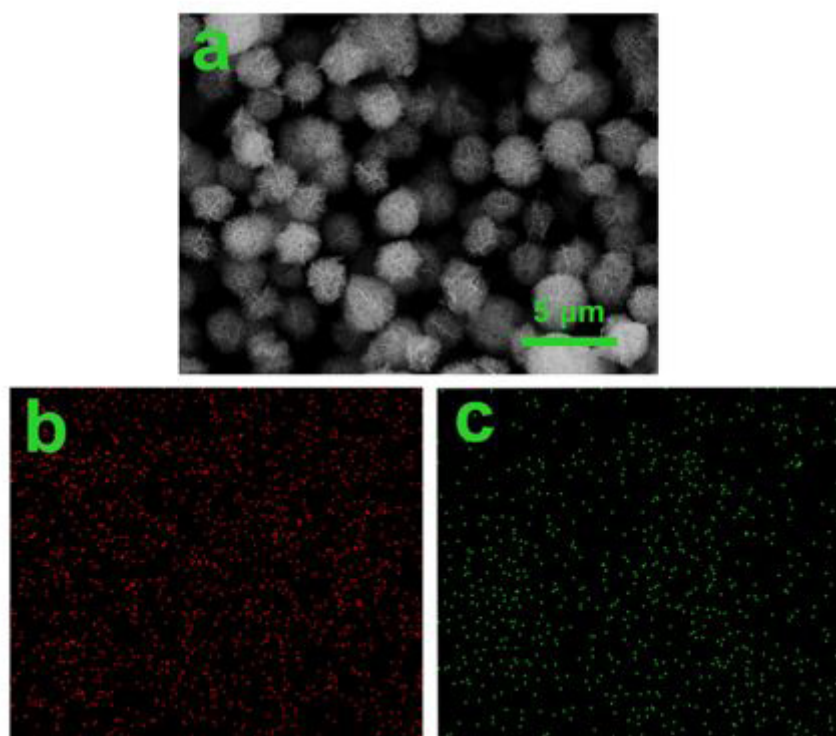**Figure 5:** XRD patterns of (a) 2 wt% Cu/F-NiO (b) 2 wt%Pd/F-NiO and (c) 2 wt% Pd$_1$Cu$_1$/F-NiO

Figure 6: (a) FE-SEM of the Pd$_1$Cu$_1$/F-NiO and EDAX mapping analysis of (b) Pd and (c) Cu in the Pd$_1$Cu$_1$/F-NiO

To get further insight into the elemental distribution in the as-prepared Pd_1Cu_1/F-NiO composite, EDAX mapping analysis of the Pd and Cu by field emission scanning electron microscopy (FE-SEM) were performed in Figure 6. The EDAX mapping analysis indicates the uniform distribution of Pd and Cu in the Pd_1Cu_1/F-NiO composite (Figure 6b and c). Furthermore, the amounts of Pd and Cu loaded on the support in these catalysts are almost identical to the results from ICP-MS analysis (Table 1).

Table 1: Pd and Cu Content (wt %) in Catalysts and the Ratio of Pd and Cu Determined by ICP-MS analysis

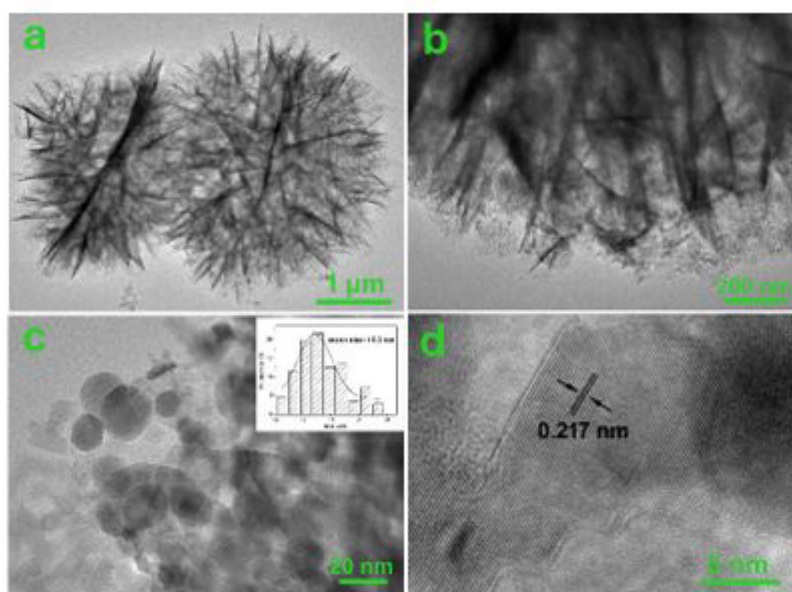| Catalyst	Pd (wt%)	Cu (wt%)	Pd:Cu (at.)
Pd /F-NiO	1.93	0	
Cu/F-NiO	0	1.85	
Pd_1Cu_1/F-NiO	1.12	0.96	1

Figure 7: TEM (a) and HRTEM (b, c) images of Pd_1Cu_1/F-NiO

To further understand the structure of F-NiO sheet and the distribution of PdCu alloy active component. The Pd_1Cu_1/F-NiO sample was performed with TEM analysis (Figure 7). It clearly reveals that the NiO sheets are actually the accumulation of nano-sized particles less than 17 nm (Figure 7b and c). The particle size and dispersion of PdCu nanoparticles could be calculated from HRTEM image, as showing in Figure 7c. The average size of PdCu from 20 particles is about 16.3 nm. Figure 7d indicates that the interplanar distance is 0.217 nm, which match with the calculated lattice parameter of PdCu alloy. These results proved the successful loading of PdCu on the NiO support. The nanosized PdCu alloy particles and the NiO support which has large BET surface area make the Pd_1Cu_1/F-NiO catalyst suitable for CO oxidation.

Figure 8 shows the CO oxidation performance for as-prepared catalysts. The flower-like NiO was also conducted in the same reaction condition for comparison. The results indicate that the pure F-NiO support show certain catalytic activity within the whole reaction temperature. It also shows that F-NiO is beneficial as support for CO oxidation. After loaded with metals, the catalytic performances of the three catalysts show significant differences. It can be seen that when Cu/F-NiO was used as the catalyst, the reaction was difficult to carry out even at 100 ^{o}C, with almost no product (4.7%) being obtained. In comparison, the Pd/F-NiO catalyst exhibited obviously enhanced catalytic activity, with the conversion reaching about 30.2% under the same reaction conditions. The above result confirmed the important role of Pd for the CO oxidation. Furthermore, when the Pd_1Cu_1/F-NiO compound was used as the catalyst, a yield of about 83.1% was achieved even at 25 ^{o}C. With a further increment of the temperature to about 150 ^{o}C, the yield would reach about 99.2%,

much higher than the other counterparts, suggesting that the synergetic effect between Pd and Cu is indeed beneficial for the progress of the reaction. All above results clearly prove that the PdCu alloy content and highly dispersion are all important for CO oxidation. NiO supported PdCu catalyst are suitable for CO elimination especially under ambient conditions.
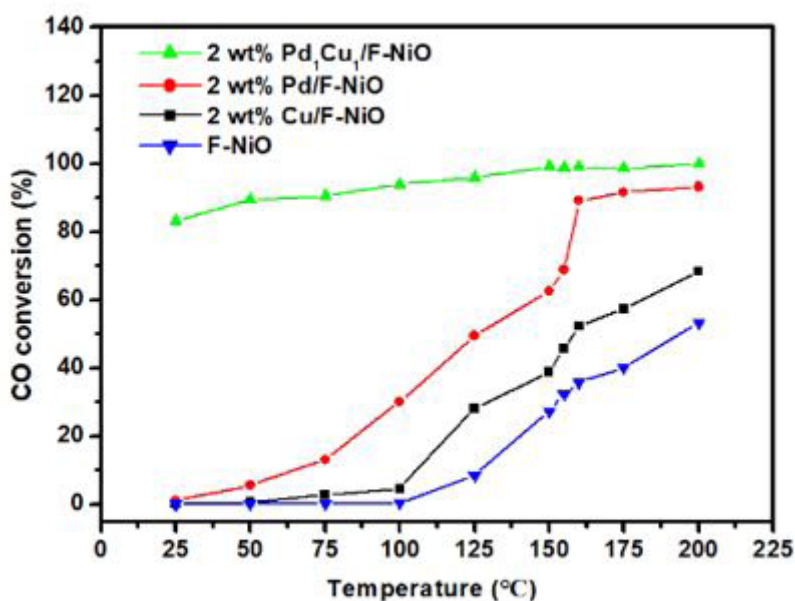

Figure 8: Catalytic performance of CO oxidation over the catalysts

To better understand the stability of Pd_1Cu_1/F-NiO, the catalyst was recovered after reaction, washed with deionized water, dried at 40°C under vacuum for 8 h and reused in a subsequent new catalytic run. As shown in Figure 9, the conversion towards CO is basically constant in the consecutive runs and only a slight decrease. This verifies that this Pd-Cu based catalyst possesses long-term stability.
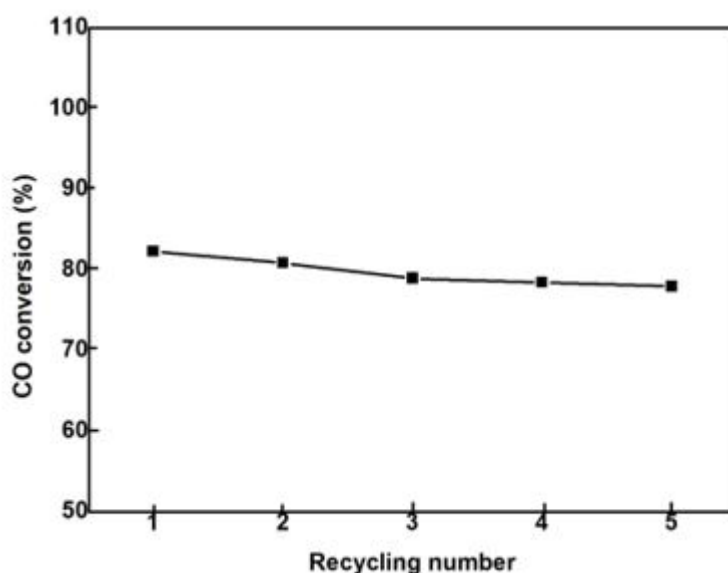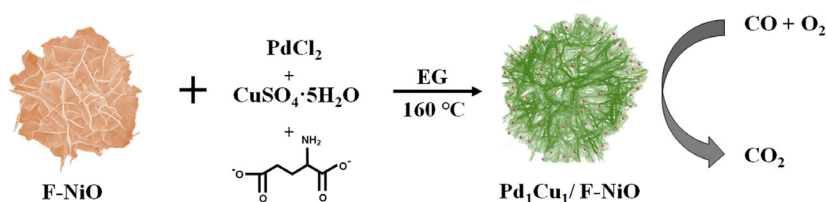

Figure 9: Pd_1Cu_1/F-NiO catalyst in the oxidation of CO. Conditions: catalyst = 100 mg; T = 25°C

Proposed Reaction Process

To better understand the formation of Pd_1Cu_1/F-NiO, a proposed reaction process is shown in Scheme 1. Firstly, F-NiO nanocrystals were successfully prepared through annealing flower-like $Ni(OH)_2 \cdot xH_2O$ precursors. Subsequently, Pd^{2+}, Cu^{2+} and glutamate were reduced by EG during the hydrothermal reaction to form PdCu nanoparticles supported F-NiO. Finally, the obtained Pd_1Cu_1/F-NiO was used for catalytic oxidation of carbon monoxide, and showed the highest catalytic activity compared with Pd/F-NiO and Cu/F-NiO.

According to many previous results [24-25], the use of intermetallic compounds by contact with active oxides may improve the catalytic properties. So, in this work, Pd_1Cu_1/F-NiO catalysts have higher catalytic oxidation of CO, which could be due to three reasons: (1) flower-like NiO possess a larger surface area, bimodal pore size distribution, higher reducibility, and superior catalytic activity for CO oxidation [26]; (2) particle size of PdCu is smaller, which is beneficial to the reaction; (3) Adding an appropriate amount of Cu can efficiently promote the surface dispersion of Pd and affect the redox properties during the CO oxidation. The particular structure of the PdCu intermetallic surface has an important role in the low kinetic barrier to the weakest adsorption strength of O_2 for the reaction, allowing for an easy approach of the O_2 dissociation and CO absorption [27-28].

Scheme 1: The reaction process of Pd_1Cu_1/F-NiO

Conclusion

In summary, hierarchically porous flower-like NiO crystals ranging from 1to 3μm have been successfully prepared through hydrothermal and pyrolysis process. NiO nanoparticles less than 10 nm aggregate together to form irregular NiO nano sheets and finally compose the flower-like NiO sphere. After decorated with PdCu alloy, the hierarchically porous structure and evenly dispersed PdCu nanoparticles make it one of the excellent catalysts for low temperature CO oxidation especially under ambient condition.

Statements and Declarations

The authors declare that they have no known competing financial interests or personal relationships that could have appeared to influence the work reported in this paper.

Acknowledgements

References

1. Mohajershojaei K, Mahmoodi NM, Khosravi A (2015) Immobilization of laccase enzyme onto titania nanoparticle and decolorization of dyes from single and binary systems. Biotechnol Biopro Eng 20: 109-116.

2. Hosseini SA, Vossoughi M, Mahmoodi NM, Sadrzadeh M (2018) Efficient dye removal from aqueous solution by high-performance electrospun nanofibrous membranes through incorporation of SiO2 nanoparticles. J Clean Prod 183: 1197-1206.

3. Masatake H, Tetsuhiko K, Hiroshi S, Nobumasa Y (1987) Novel Gold Catalysts for the Oxidation of Carbon Monoxide at a Temperature far Below 0 °C. Chem lett 16: 405-408.

4. Wang HF, Kavanagh R, Guo YL, Guo Y, Lu GZ, Hu P (2012) Structural Origin: Water Deactivates Metal Oxides to CO Oxidation and Promotes Low-Temperature CO Oxidation with Metals. Angew Chem Int Ed 51: 6657-6661.

5. Xie X, Li L, Liu ZQ, Haruta M, Shen WJ (2009) Low-temperature oxidation of CO catalysed by Co (3) O (4) nanorods. Nature 458:746-749.

6. Cao JL, Wang Y, Sun G, Zhang ZY (2011) CuO/Ce x Sn1-x O2 catalysts: Synthesis, characterization, and catalytic performance for low-temperature CO oxidation. Trans Metal Chem 36: 107-112.

7. Zhang Y, Li G, Tana L, Liu L, Li Y, Li Liang (2017) Appl Surf Sci 423: 961-967

8. Zhao B, Ke Xg, Bao J, Wang C, Dong L, Chen Y Chen H (2009) Synthesis of Flower-Like NiO and Effects of Morphology on Its Catalytic Properties. J Phys Chem C 113: 14440–14447.

9. Rastegarpanah A, Liu Y, Deng J, Jing L, Pei W, Zhang X, Hou Z, Rezaei M, Dai, H (2021) 297: 122091-122099

10. Wang X, Li L, Zhang YG, Wang ST, Zhang ZD, Fei LF, Qian YT (2006) Cryst Growth Des 6: 2163-2165

11. Wang C, Wang D, Wang Q, Chen H (2010) J Power Sour 195:7432–7437.

12. Chatterjee S, Maiti R, Chakravorty D (2020) Large magnetodielectric effect and negative magnetoresistance in NiO nanoparticles at room temperature. RSC Adv 10:13708-13716.

13. Saoud KM, El-Shall MS (2020) Catal 10:1351-1371.

14. McCrea KR, Parker JS, Somorjai GA (2002) J Phys Chem B 106:10854-10863.

15. Camposeco R, Castillo S, Hinojosa-Reyes M, Zanella R, Lopez-Curiel JC, Fuentes GA, Mejia-Centeno I (2019) Catal Lett 149: 1565-1578.

16. Ivanova AS, Slavinskaya EM, Stonkus OA, Gulyaev RV, Glazneva TS, Noskova AS, Boronin AI (2016) Catal Sci Technol 6: 3918-3928.

17. Li G, Li L, Jiang D, Shi J (2015) Electrospun hollow ZnO/NiO heterostructures with enhanced photocatalytic activity. RSC Adv 5: 40352-40357.

18. Al-Soubaih R, Saoud KM, Myint, MTZ, Goethelid MA, Dutta J (2021) Co oxidation efficiency and hysteresis behavior over mesoporous pd/sio2 catalyst. Catal 11: 131-148.

19. Watanabe M, Zhu Y, Uchida H (2000) Oxidation of CO on a Pt−Fe Alloy Electrode Studied by Surface Enhanced Infrared Reflection−Absorption Spectroscopy. J Phys Chem B 104: 1762-1768.

20. Komatsu T, Tamura A (2008) Pt3Co and PtCu intermetallic compounds: Promising catalysts for preferential oxidation of CO in excess hydrogen. J Catal 258: 306-314.

21. Castillo R, Dominguez Garcia E, Santos JL, Centeno MA, Romero Sarria F, Daturib M, Odriozola JA (2020) Upgrading the PtCu intermetallic compounds: The role of Pt and Cu in the alloy. Catal Today 356:390-398

22. Oveisia M, Mahmoodi NM, Aslia MA (2019) J Clean Prod 222: 669-684.

23. Mahmoodi NM, Taghizadeh A, Taghizadeh M, Abdi J (2019) In situ deposition of Ag/AgCl on the surface of magnetic metal-organic framework nanocomposite and its application for the visible-light photocatalytic degradation of Rhodamine dye. J Hazard Mater 378: 120741.

24. Suárez JA, Plata JJ, Márquez AM, Sanz JF (2022) Catal Today 383:339-343.

25. Zhang W, Shan S, Luo J, Fisher A, Chen JF, Zhong CJ, Zhu J, Cheng D (2017) J Phys Chem C 121: 11010–11020

26. Zhao B, Ke XK, Bao JH, Wang CL, Dong L, Chen YW, Chen HL (2009) Synthesis of Flower-Like NiO and Effects of Morphology on Its Catalytic Properties. J Phys Chem C 113: 14440-14447.

27. Li YY, Hu J, Chen MS, Wan HL (2022) J Phys Chem C 126:1420-1425.

28. Zhang W, Shan SY, Luo J, Fisher A, Chen JF, Zhong CJ, Zhu JQ, Cheng DJ (2017) J Phys Chem C 121: 11010–11020.